THE JOURNAL OF BIOLOGICAL CHEMISTRY VOL. 288, NO. 7, pp. 4947–4956, February 15, 2013

Ablation of Ceramide Synthase 2 Causes Chronic Oxidative Stress Due to Disruption of the Mitochondrial Respiratory Chain*

Received for publication, July 19, 2012, and in revised form, December 11, 2012 Published, JBC Papers in Press, January 2, 2013, DOI 10.1074/jbc.M112.402719

Hila Zigdon[‡1], Aviram Kogot-Levin[§1], Joo-Won Park[‡2], Ruth Goldschmidt[¶], Samuel Kelly[‖], Alfred H. Merrill, Jr.[‖], Avigdor Scherz[¶3], Yael Pewzner-Jung[‡], Ann Saada[§], and Anthony H. Futerman[‡4]

From the Departments of [‡]Biological Chemistry and [¶]Plant Sciences, Weizmann Institute of Science, Rehovot 76100, Israel, the [§]Monique and Jacques Roboh Department of Genetic Research, Department of Genetics and Metabolic Diseases, Hadassah, Hebrew University Medical Center, 91120 Jerusalem, Israel, and [‖]School of Biology and Petit Institute for Bioengineering and Bioscience, Georgia Institute of Technology, Atlanta, Georgia 30332-0230

Background: Ceramide synthase 2 null mice, which cannot synthesize very-long chain ceramides, display severe hepatopathy.
Results: These mice have elevated sphinganine and altered *N*-acyl chain ceramides that disrupt mitochondrial function by modifying respiratory chain activity.
Conclusion: Alteration of mitochondrial sphingolipids results in formation of reaction oxygen species in liver.
Significance: Ceramides with defined acyl chains influence oxidative stress signaling pathways.

Ceramide is a key intermediate in the pathway of sphingolipid biosynthesis and is an important intracellular messenger. We recently generated a ceramide synthase 2 (CerS2) null mouse that cannot synthesize very long acyl chain (C22-C24) ceramides. This mouse displays severe and progressive hepatopathy. Significant changes were observed in the sphingolipid profile of CerS2 null mouse liver, including elevated C16-ceramide and sphinganine levels in liver and in isolated mitochondrial fractions. Because ceramide may be involved in reactive oxygen species (ROS) formation, we examined whether ROS generation was affected in CerS2 null mice. Levels of a number of anti-oxidant enzymes were elevated, as were lipid peroxidation, protein nitrosylation, and ROS. ROS were generated from mitochondria due to impaired complex IV activity. C16-ceramide, sphingosine, and sphinganine directly inhibited complex IV activity in isolated mitochondria and in mitoplasts, whereas other ceramide species, sphingomyelin, and diacylglycerol were without effect. A fluorescent analog of sphinganine accumulated in mitochondria. Heart mitochondria did not display a substantial alteration in the sphingolipid profile or in complex IV activity. We suggest that C16-ceramide and/or sphinganine induce ROS formation through the modulation of mitochondrial complex IV activity, resulting in chronic oxidative stress. These results are of relevance for understanding modulation of ROS signaling by sphingolipids.

Ceramide, a key intermediate in the pathway of sphingolipid (SL)[5] metabolism (1–4), is synthesized by a family of ceramide synthases (CerS), each of which adds acyl chains of defined length to the sphingoid long chain base (5, 6). Major advances concerning the biological role of the CerS and of the ceramide species that they generate have been obtained from studies using genetically modified mice in which one of the CerS genes has been ablated. A CerS1 null mouse displays cerebellar Purkinje cell neurodegeneration due to reduced levels of C18-ceramide (7, 8), and a CerS3 null mouse displays defects in the skin barrier due to loss of ultralong-chain (>C26) ceramides (9).

We recently generated a CerS2 null mouse that lacks C22-C24-ceramides with a concomitant elevation by an as-yet unknown mechanism of C16-ceramide and sphinganine in liver (10). This mouse displays severe hepatopathy (11) and hepatic insulin resistance (12), defects in myelin in the central nervous system (13), and a number of pronounced biophysical changes in the properties of membrane lipids (14, 15).

The hepatopathy of CerS2 null mice is characterized by a number of features, including enhanced hepatocyte apoptosis and proliferation (11). High throughput RNA expression analysis in liver revealed up-regulation of genes associated with cell cycle regulation, protein transport, cell-cell interactions and apoptosis, and down-regulation of genes associated with intermediary metabolism such as lipid and steroid metabolism, adipocyte signaling, and amino acid metabolism (11). In addition, significant changes were observed in levels of genes associated with anti-oxidant activity (16–18) by 2 weeks of age (Table 1), suggesting that reactive oxygen species (ROS) might play a role in hepatopathy.

* This work was supported, in whole or in part, by National Institutes of Health Grant GM076217. This work was also supported by the Israel Science Foundation (0888/11) and the Minerva Foundation.
[1] Both authors contributed equally to this study.
[2] Present address: Dept. of Biochemistry, School of Medicine, Ewha Womans University, Seoul 158-710, South Korea.
[3] The Robert and Yadelle Sklare Professor of Biochemistry at the Weizmann Institute of Science.
[4] The Joseph Meyerhoff Professor of Biochemistry at the Weizmann Institute of Science. To whom correspondence should be addressed. Tel.: 972-8-9342704; Fax: 972-8-9344112; E-mail: tony.futerman@weizmann.ac.il.

[5] The abbreviations used are: SL, sphingolipid; CerS, ceramide synthase; NBD, 4-nitrobenzo-2-oxa-1,3-diazole; ROS, reactive oxygen species; RNS, reactive nitrogen species; 4-HNE, 4-hydroxynonenal; H_2DCF-DA, 6-carboxy-2′,7′-dichlorodihydrofluorescein diacetate; DAF-FM, 4-amino-5-methylamino- 2′,7′-difluorescein.

TABLE 1

mRNA expression levels of anti-oxidant enzymes

Digital gene expression analysis of anti-oxidant enzymes in liver is shown. The data are taken from the EntrezGene ID gene list from the supplementary material in Pewzner-Jung *et al.* (11). Results are -fold change of mRNA levels of CerS2 null mice *versus* WT, $n = 3$; p values are in parentheses.

Protein	Gene annotation	-Fold change (null versus WT)	
		14 days old	30 days old
Glutathione peroxidase 4	Gpx4	ND[a]	2.27 (<0.1)
Glutathione peroxidase 7	Gpx7	1.54 (<0.05)	2.56 (<0.005)
Glutathione peroxidase 3	Gpx3	5.62 (<0.001)	6.46 (<0.001)
Glutathione S-transferase mu 1	Gstm1	2.29 (<0.05)	2.32 (<0.001)
Glutathione S-transferase pi 1	Gstp1	ND	4.60 (<0.001)
Superoxide dismutase 1, soluble	Sod1	ND	1.86 (<0.001)

[a] Not detected.

ROS are a variety of molecules and free radicals derived from molecular oxygen (19). ROS affect cellular function in either a positive or negative fashion, depending on the cell type and on the intensity and the duration of the exposure (19–21). The superoxide anion (O_2^-) is the precursor of most ROS and a mediator in most oxidative chain reactions. The mitochondrial electron transport chain contains several redox centers that may leak electrons to O_2, constituting the primary source of O_2^- in most tissues (19).

A link between SL metabolism and ROS generation has been reported (22–25). We now analyze ROS production in CerS2 null mouse liver. ROS levels were elevated along with a reduction in mitochondrial membrane potential. Furthermore, mitochondrial respiratory chain dysfunction was observed due to the impairment of complex IV activity by C16-ceramide and sphinganine. Our data are consistent with the notion that ceramides with defined acyl chain lengths impact down-stream signaling pathways in which ROS are involved.

EXPERIMENTAL PROCEDURES

Materials—The following antibodies were used: anti-nitrotyrosine (Abcam), anti-glyceraldehyde 3-phosphate dehydrogenase (GAPDH) (Millipore), anti-4-hydroxynonenal (HNE)-Michael adduct (Calbiochem), and goat anti-rabbit peroxidase-conjugated (HRP) secondary antibody (Jackson ImmunoResearch). 4-Nitrobenzo-2-oxa-1,3-diazole (NBD)-sphinganine was from Avanti Polar Lipids, Alabaster, AL.

Mice—WT and CerS2 null mice were maintained in a constant atmosphere under special pathogen-free conditions. Experimental protocols were approved by the Institutional Animal Care and Use Committee of the Weizmann Institute of Science. Mice were sacrificed using CO_2. Livers were harvested and transferred to either liquid nitrogen or a fixative agent.

RNA Extraction and Polymerase Chain Reaction—Total RNA was isolated using the RNeasy mini kit (Qiagen) according to the manufacturer's instructions, which included the addition of β-mercaptoethanol. cDNA synthesis was performed using a Verso cDNA kit (Thermo Scientific). RT-PCR was performed using a SYBR Green PCR reaction master mix (Finnzyme) and an ABI Prism 7000 Sequence Detection System (Applied Biosystems). The primer concentration was 1 nM in a reaction volume of 20 μl. Each reaction was performed in duplicate. The thermal cycling parameters were as follows: step 1, 50 °C for 2 min; step 2, 95 °C for 10 min; step 3, 95 °C for 15 s, 60 °C for 1 min. Step 3 was repeated for 40 cycles and was followed by a dissociation step. The relative amounts of mRNA were calculated from the cyclic threshold values using hypoxanthine-guanine phosphoribosyltransferase (HPRT) or TATA binding protein (TBP) for normalization. Normalization was assessed using geNorm software. Results are presented as mean of -fold -change of mRNA levels in experimental samples *versus* controls samples. Primers are given in Table 2.

Electron Spin Resonance—ESR measurements were performed using a Magnettech Miniscope MS100 spectrometer equipped with a microwave X-band bridge. The spectrometer operates at 9.3–9.55 GHz and 20-milliwatt microwave. Ten minutes before collection of blood, mice were injected intravenously with 4-phosphono-oxy-2,2,6,6-tetramethylpiperidine-*N*-hydroxyl (75 μg/kg). Blood was drawn from the heart under ketamine:xylazine anesthesia and measured immediately using glass capillaries.

Immunohistochemistry—Livers were fixed in 4% paraformaldehyde for 2 days and then embedded in paraffin. Paraffin sections (4-μm thick) were deparaffinized, and endogenous peroxidase activity was blocked by treating with 0.3% (v/v) hydrogen peroxide and 0.5% (v/v) HCl in methanol for 30 min. Antigen retrieval was performed using 10 mM citric acid (pH 6.0) for 10 min. To reduce the nonspecific signal, sections were blocked using 20% (v/v) normal horse serum (Vector Laboratories) and 0.2% (v/v) Triton X-100 for 2 h. Sections were incubated with an anti-HNE-Michael adduct antibody at a dilution of 1:300 in 2% (v/v) normal horse serum and 0.1% (v/v) Triton X-100 overnight at 4 °C. After several rinses in PBS, tissue sections were incubated with a goat anti-rabbit peroxidase-conjugated (HRP) secondary antibody at a 1:200 dilution in 2% (v/v) normal horse serum and 0.1% (v/v) Triton X-100 for 1 h at room temperature. Peroxidase activity was detected by incubation with 3,3′-diaminobenzidine for 10 min. Sections were rinsed in distilled H_2O, counterstained with hematoxylin, rinsed again under running tap water, and covered with coverslips using Entellan (Merck) as mounting agent.

Lipid Peroxidation—Lipid peroxidation in liver homogenates was determined by measuring levels of hydroxynonenal-histidine (HNE-His) protein adducts, which were quantified using the Oxiselect HNE-His Adduct ELISA kit (Cell Biolabs, Inc.). Protein samples were adsorbed onto a 96-well plate. HNE-protein adducts were probed with an anti-HNE-His antibody followed by an HRP-conjugated secondary antibody. Levels of HNE-protein adducts were determined using a standard curve prepared from a predetermined HNE-bovine serum albumin standard.

TABLE 2
Primers used for RT-PCR
F, forward; R, reverse.

Gene	Primers	Reference
Gsta1	F, 5′-CGCCACCAAATATGACCTCT-3′ R, 5′-TTGCCCAATCATTTCAGTCA-3′	
Gstm3	F, 5′-CACCCGCATACAGCTCATGAT-3′ R, 5′-TTCTCAGGGATGGCCTTCAA-3′	58
Hprt1	F, 5′-TGCTCGAGATGTCATGAAGG-3′ R, 5′-AATCCAGCAGGTCAGCAAAG-3′	59
TBP	F, 5′-TGCTGTTGGTGATTGTTGGT-3′ R, 5′-CTGGCTTGTGTGGGAAAGAT-3′	

Protein Extraction and Western Blotting—Liver tissues were lysed in ~6 volumes of PBS supplemented with a protease inhibitor mixture (Sigma). Tissues were homogenized by sonication. Protein was quantified using the BCA reagent (Pierce). Fifty μg of protein was electrophoresed on a 12% SDS-polyacrylamide gel and transferred to a nitrocellulose membrane. Blots were incubated with primary antibodies followed by a horseradish peroxidase-conjugated secondary antibody. Bound antibodies were detected using the SuperSignal West Pico chemiluminescent substrate (Thermo Scientific).

Mouse Hepatocyte Cultures—Hepatocytes were isolated as described with some modifications (26, 27). Mice were perfused through the inferior vena cava with Hanks' buffered salt solution containing 5 mM KCl, 5 mM glucose, 25 mM $NaHCO_3$, and 0.4 mM EDTA preheated to 42 °C. Perfusion was performed using a peristaltic pump at a rate of 4 ml/min for 4 min. The buffer was immediately replaced with liver digest media (Invitrogen) preheated to 42 °C for 12 min. The liver was collected in 10 ml of plating medium (DMEM supplemented with 10% fetal bovine serum, 2 mm sodium pyruvate, 2% penicillin/streptomycin, 1 μm dexamethasone, and 0.1 μm insulin). The liver was dissected using tweezers and passed through a cell strainer (70-μm nylon). Cells were centrifuged at 50 $\times$ g_{av} (5 min, 4 °C). The pellet was resuspended in 50% Percoll in plating medium. After centrifugation, dead cells were removed, and the pellet was washed twice using plating medium. Cells were seeded at a density of 5×10^5 cells/1.5 ml in collagen-coated 6-well plates. The hepatocytes anchored to the dishes within 2 h. Medium was replaced 2 h after plating with DMEM supplemented with 0.2% BSA, 2 mM sodium pyruvate, 2% penicillin/streptomycin, 0.1 μM dexamethasone, and 1 nM insulin. Culture dishes were maintained at 37 °C in a 5% CO_2-humidified incubator. In some experiments hepatocytes were incubated with ascorbic acid (4 mM) for 18 h.

ROS and Reactive Nitrogen Species—ROS and reactive nitrogen species (RNS) were measured using 6-carboxy-2′,7′-dichlorodihydrofluorescein diacetate (H_2DCF-DA) (Invitrogen) and 4-amino-5-methylamino-2′,7′-difluorescein (DAF-FM) (Invitrogen), respectively. Hepatocytes were incubated with 100 μM concentrations of either probe in PBS for 30 min at 37 °C. Cells were washed 3 times and incubated with PBS for an additional 3 h. Cells were detached from the plates using trypsin-EDTA, centrifuged at 250 $\times$ g_{av} for 5 min, and resuspended in PBS. Conversion of the non-fluorescent H_2DCF-DA to DCF and DAF-FM to benzotriazole was monitored by FACS (BD Biosciences) at an excitation wavelength of 495 nm and an emission wavelength of 530 nm.

SL Analysis—SL analyses by electrospray ionization-tandem mass spectrometry were conducted using a PE-Sciex API 3000 triple quadrupole mass spectrometer and an ABI 4000 quadrupole-linear ion trap mass spectrometer (28–31).

Isolation of Enriched Mitochondrial Fractions—Liver was minced on ice and homogenized using a Teflon glass homogenizer at 250 rpm in 250 mM sucrose, 2 mM EDTA, 10 mM Tris (pH 7.4), and 50 IU heparin (SETH buffer). Homogenates were centrifuged at 1000 $\times$ g_{av} (10 min, 4 °C). The supernatant was collected, transferred to clean tubes, and centrifuged at 14,000 $\times$ g_{av} (15 min, 4 °C). The mitochondrial pellet was washed at 14,000 $\times$ g_{av} and resuspended in a small volume of SETH buffer (32), aliquotted, and stored at −70 °C. Protein was determined by the Lowry method (33).

Mitoplast Preparation—Mitoplasts were prepared from isolated liver mitochondria using 0.2% digitonin as described (34).

Mitochondrial ROS Production—Mitochondrial ROS production was determined spectrofluorometrically using H_2DCF-DA (35). Mitochondria (0.25 mg of protein/ml) were incubated at 30 °C with 2 μM H_2DCF-DA and 10 mM succinate. DCF fluorescence was monitored using a Synergy HT microplate reader (Bio-Tek Instruments, Vinoosky, VT) at an excitation wavelength of 485 nm and emission wavelength of 520 nm.

Respiratory Chain Enzymes—Citrate synthase, rotenone sensitive NADH coenzyme Q reductase (complex I), succinate dehydrogenase (complex II), succinate cytochrome *c* reductase (complex II + III), and cytochrome *c* oxidase (complex IV) were determined in isolated liver mitochondria using standard spectrophotometric methods (36). When assaying the effect of sphinganine and ceramides, the lipids or vehicle were added to the assay buffer and preincubated with the mitochondria for 5 min at 37 °C. All lipids were dissolved in ethanol or ethanol: dodecane (98:2, v/v); the solvents themselves had no effect.

Mitochondrial Membrane Potential—Mitochondrial membrane potential ($\Delta\psi$m) was estimated using JC-1 (Invitrogen) (37). Hepatocytes were incubated with 0.4 μM JC-1 in maintenance media for 15 min at 37 °C. Cells were detached from the plates using trypsin-EDTA, centrifuged at 250 $\times$ g_{av} for 5 min, and resuspended in PBS. Quantification was performed by FACS (BD Biosciences) at an excitation wavelength of 498 nm and an emission wavelength of 535 nm (for green fluorescence) and at an excitation wavelength of 560 nm and an emission wavelength of 590 nm (for red fluorescence).

NBD-Sphinganine Labeling—Human skin fibroblasts were grown on 25-mm glass coverslips in DMEM supplemented with 20% fetal bovine serum. Cells were fixed with 0.5% glutaraldehyde for 10 min at room temperature, washed 3 times with DMEM, and incubated for 30 min at 4 °C with 5 μM NBD-sphinganine complexed with defatted bovine serum albumin. After incubation, cells were washed with DMEM. Background fluorescence was reduced by incubation four times with 3.4 mg of defatted bovine serum albumin/ml DMEM at 4 °C followed by washing in PBS (38). Cells were incubated with 2 μM Mitotracker red (Invitrogen) before fixation. Glass coverslips were mounted on slides and observed by fluorescence microscopy (Olympus BXUCB).

Statistics—*p* values were calculated using a two-tailed unpaired samples Student's *t* test.

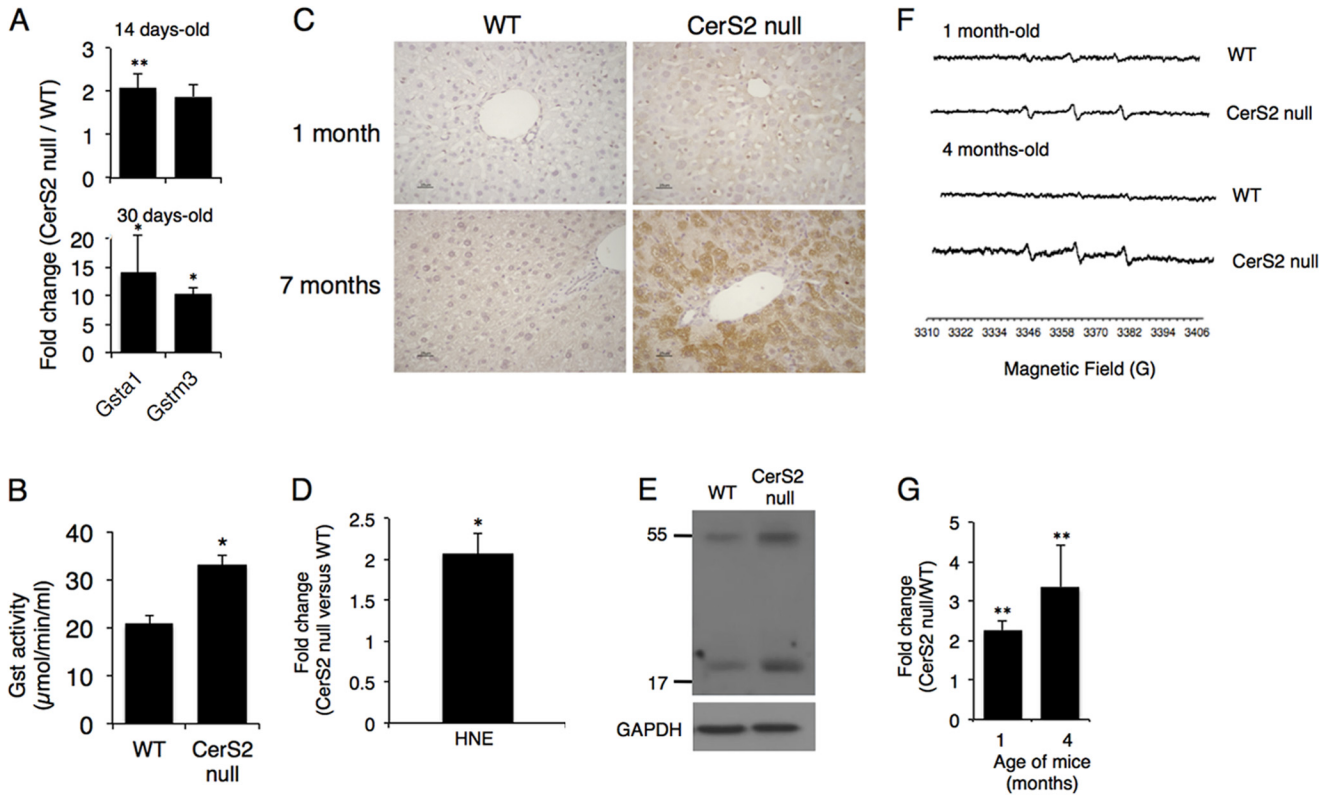

FIGURE 1. **Oxidative stress markers in CerS2 null mouse.** *A*, quantitative real-time-PCR analysis of Gst isozymes in liver is shown. Results are fold-change of mRNA levels of CerS2 null mice *versus* WT at the indicated ages. Values are the means ± S.D., $n = 3$. *, $p < 0.05$; **, $p < 0.01$. *B*, Gst activity in 1-month-old mouse liver is shown. Values are the means ± S.D., $n = 3$. *, $p < 0.05$. *C*, immunohistochemical staining of 4-HNE is shown. *Scale bar* = 25 μm. *D*, shown are 4-HNE levels in 4 month-old mice liver. Values are the means ± S.D., $n = 3$. *, $p < 0.05$. *E*, shown is a Western blot of nitrotyrosine in livers of 4-month-old mice liver. GAPDH was used as loading control. Results are from a typical experiments repeated three times. *F*, shown are representative ESR spectra of 4-phosphono-oxy-2,2,6,6-tetramethyl-piperidine-*N*-hydroxyl-radical adducts in the blood of 1-month- and 4-month-old mice. *G*, shown is quantification of amplitude intensity ($n = 2$ for 1-month-old and $n = 2$ for 4-month-old). *, $p < 0.01$.

RESULTS

Elevated Oxidative Stress in CerS2 Null Mice—To examine the levels of anti-oxidant gene expression in CerS2 null mouse liver, mRNA expression of two members of the Gst family (16–18) was analyzed by RT-PCR. An ~10-fold increase in Gsta1 and Gstm3 was observed in 30-day-old mice, with a smaller elevation in 14-day-old mice (Fig. 1*A*). Gst activity increased by 1.5-fold in 1-month-old mice (Fig. 1*B*).

Lipid peroxidation occurs upon free radical attack on the unsaturated bonds of membrane fatty acids leading to formation of reactive compounds such as 4-HNE (39, 40). In liver sections taken from 1- and 7-month-old mice, cytoplasmic labeling of HNE was detected in CerS2 null but not in WT mice (Fig. 1*C*). Similar results were obtained by ELISA (Fig. 1*D*). Nitrotyrosine levels were also elevated in 4-month-old CerS2 null mice (Fig. 1*E*) and in some livers of 1-month-old mice (data not shown). We conclude that significant oxidative damage occurs in the liver of CerS2 null mice.

To determine if changes in anti-oxidant gene expression correlate with ROS elevation, levels of free radicals were examined by ESR using 4-phosphono-oxy-2,2,6,6-tetramethyl-piperidine-*N*-hydroxyl (PPH) as a spin trap for hydroxyl and superoxide free radicals. An ~2–3-fold increase in signal amplitude was observed in CerS2 null mice at 1 and 4 months of age (Fig. 1, *F* and *G*), demonstrating that ROS accumulate in the blood of CerS2 null mice and cause chronic oxidative stress, which may be the cause of the increase in anti-oxidant-protective mechanisms.

Role of Mitochondria and the Mitochondrial Respiratory Chain in ROS Generation in CerS2 Null Mice—To determine whether hepatocytes are the source of free radicals, ROS and RNS were measured in isolated hepatocytes. ROS (Fig. 2*A*) and RNS (Fig. 2*B*) were significantly elevated in hepatocytes from 2.5-month-old CerS2 null mice. ROS formation was also elevated in isolated liver mitochondria (Fig. 3), consistent with the notion (19, 24) that the mitochondrial electron transport chain is the primary source of ROS.

We next analyzed the activity of electron transport chain complexes I-IV in isolated liver mitochondria fractions. Activities were normalized to citrate synthase activity, as citrate synthase activity was similar in CerS2 null mice mitochondria compared with WT (315 ± 52 *versus* 306 ± 60, respectively). No changes were observed in the activity of complexes I and III, but a partial reduction in complex II and a marked reduction in complex IV activity were detected in mitochondria from 1-month-old CerS2 null mice (Fig. 4*A*). A reduction in complex IV activity was also detected in cultured hepatocytes (Fig. 4*B*).

Mitochondrial membrane potential ($\Delta\psi m$) was impaired in CerS2 null hepatocytes (Fig. 5*A*). Three antioxidants, ascorbic acid, α-tocopherol, and *N*-acetyl-L-cysteine, were incubated with hepatocytes. Ascorbic acid was most effective in reducing ROS levels (Fig. 5*B*), but despite this reduction, mitochondrial

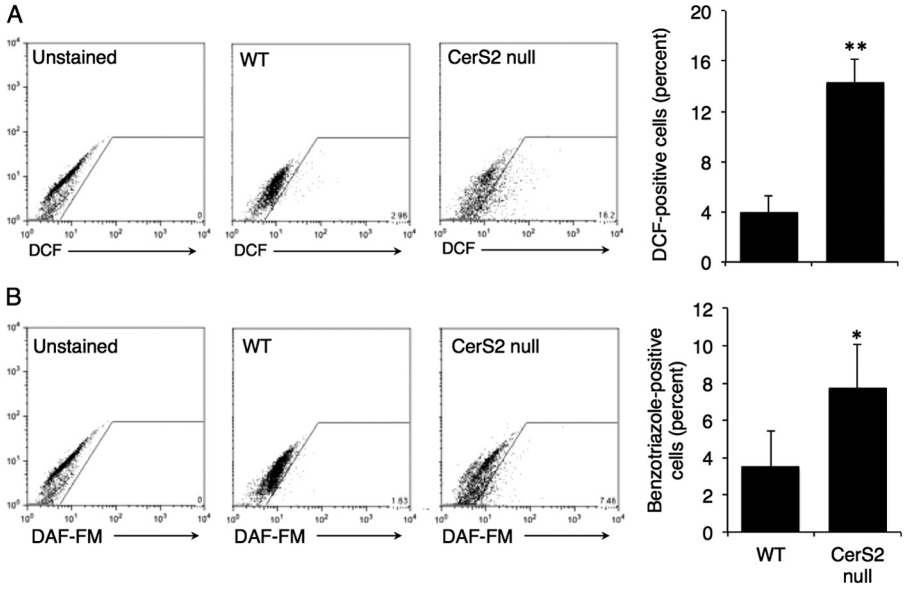

FIGURE 2. **ROS and RNS levels in CerS2 null mouse hepatocytes.** Representative and quantified FACS analysis of ROS levels using H_2DCF-DA (*A*) and RNS levels (*B*) using DAF-FM. Values are the means ± S.D., $n = 3$. *, $p < 0.05$, **, $p < 0.01$.

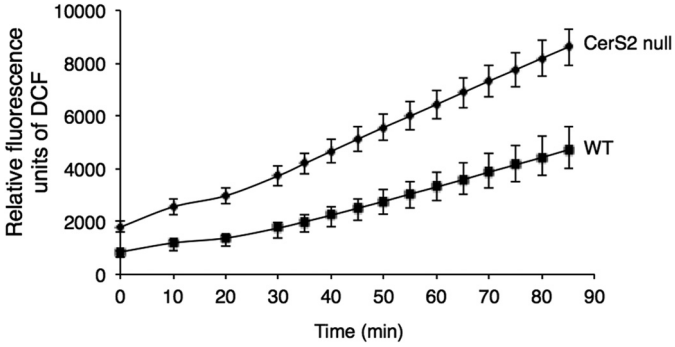

FIGURE 3. **ROS levels in isolated mitochondria from CerS2 null mice.** ROS levels were measured by DCF fluorescence. Values are means ± S.D., $n = 3$.

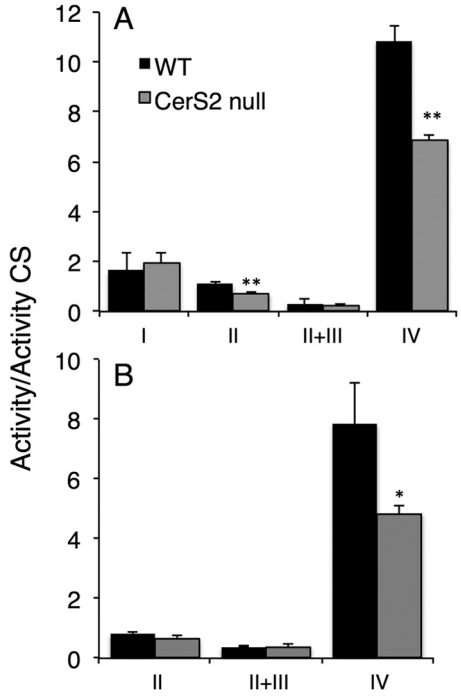

FIGURE 4. **Enzymatic activities of mitochondrial respiratory complexes.** Activities of mitochondrial complexes normalized to citrate synthase (*CS*) in liver mitochondria obtained from 1-month-old mice (*A*) and hepatocytes isolated from 2.5-month-old mouse liver (*B*) are shown. Activities are normalized to citrate synthase. Values are the means ± S.D. $n = 3$. *, $p < 0.05$. **, $p < 0.01$.

membrane potential was unaltered (Fig. 5*C*), implying that ROS are not the primary cause of mitochondrial membrane potential impairment in CerS2 null hepatocytes.

Analysis of the sphingolipid profile in the same mitochondrial fractions used to assay the activity of the electron transport chain complexes and to assay mitochondrial membrane potential demonstrated similar changes to those observed in whole liver (10). Thus, levels of C22-C24-ceramide were barely detectable, whereas levels of C16-ceramide were significantly elevated (Fig. 6*A*). Similarly, sphingosine and sphinganine levels were elevated by ~2- and ~50-fold, respectively (Fig. 6*B*).

To gain mechanistic insight into the mode of mitochondrial dysfunction, the effect of exogenously added SLs on complex IV activity was examined in isolated mitochondria from WT mice. Remarkably, C16-ceramide, sphingosine, and sphinganine, which accumulate in CerS2 null mouse liver (10), each inhibited complex IV activity, and an additive effect was observed when they were added together (Fig. 7*A*). Neither C24:0- nor C24:1-ceramide had any effect on complex IV activity. C16-sphingomyelin, which is also elevated in mitochondrial fractions (data not shown), had a small but statistically insignificant inhibitory effect on complex IV activity. Moreover, C16:0-C18:1-diacylglycerol, which is similar in its hydrophobic properties to C16-ceramide, had no effect on complex IV activity (Fig. 7*A*). None of the exogenously added lipids affected complex IV activity in mitochondria from CerS2 null mice (Fig. 7*B*), suggesting maximal inhibition of complex IV activity in CerS2 null mouse liver mitochondria. Similar results were obtained in mitoplasts (Fig. 7*C*). Together, these results demonstrate that ROS generation is caused by direct inhibition of complex IV activity by two of the lipids that accumulate in CerS2 null mice liver, namely C16:0-ceramide and sphinganine.

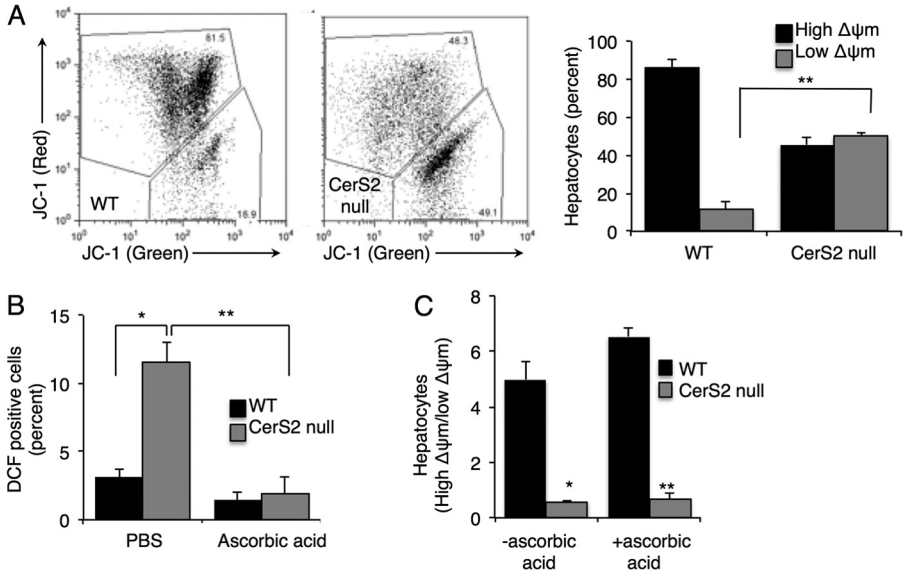

FIGURE 5. **Mitochondrial membrane potential in hepatocytes.** *A*, shown is a representative FACS analysis of mitochondrial membrane potential estimated using JC-1. The percent of hepatocytes with low ΔΨm was calculated from the lower gate. $n = 4$. *B*, shown are ROS levels after PBS or ascorbic acid treatment. *C*, mitochondrial membrane potential after ascorbic acid treatment is shown. Values are the means ± S.E., $n = 3–6$. *, $p < 0.01$; **, $p < 0.001$.

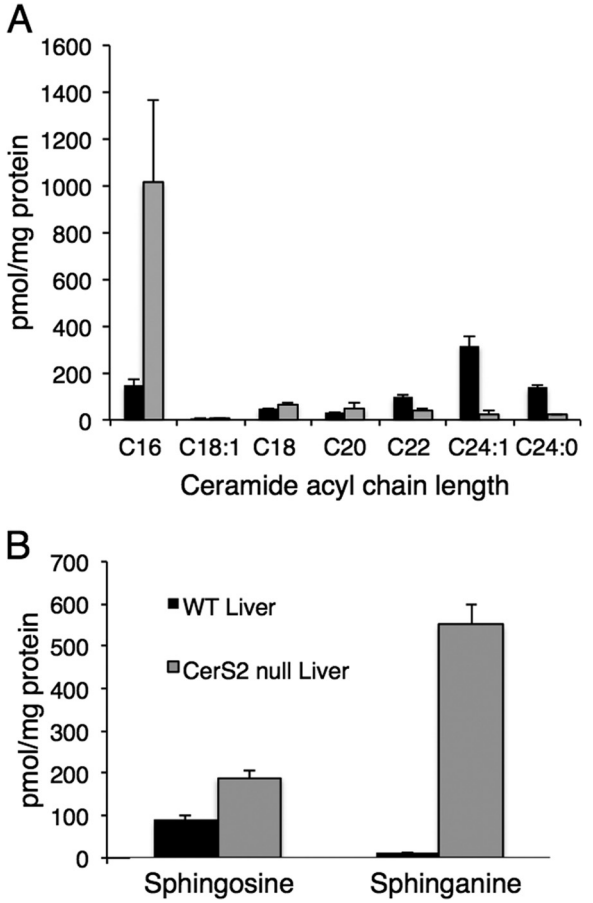

FIGURE 6. **SL profile of a liver mitochondrial fraction.** Mass spectrometry analysis of ceramide acyl chain length (*A*) and sphingosine and sphinganine levels (*B*) in a mitochondrial fraction isolated from liver is shown. Values are the means ± S.D., $n = 4$.

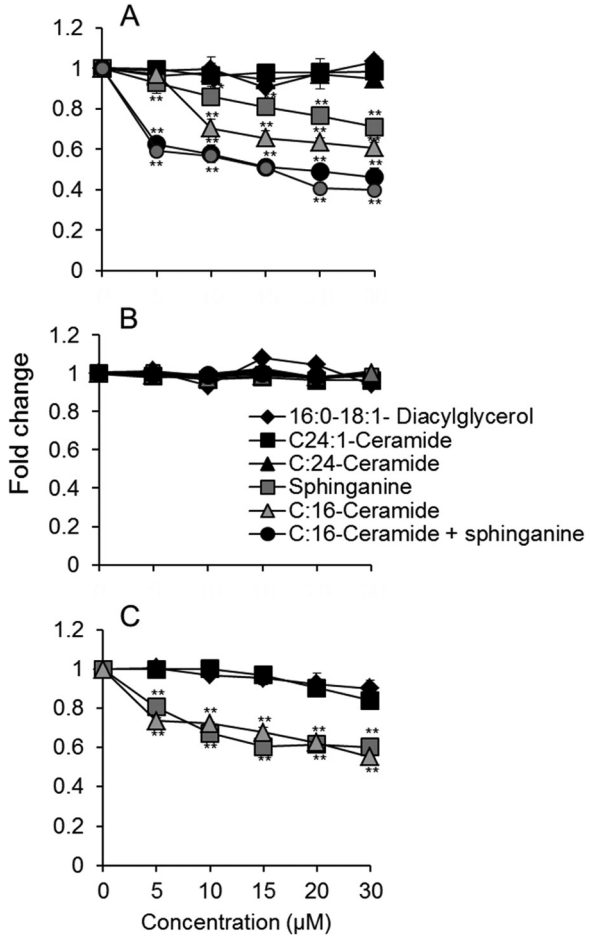

FIGURE 7. **Effect of sphinganine, sphingosine, and ceramides on mitochondrial complex IV activity.** Complex IV activity was measured in mitochondria isolated from the liver of 2-month-old WT mice (*A*), mitochondria from the liver of 2 month-old CerS2 null mice (*B*), and mitoplasts from WT mice (*C*). Values are means ± S.D. $n = 3$. **, $p < 0.01$.

To examine whether sphinganine is able to accumulate in mitochondria, human skin fibroblasts were incubated with NBD-sphinganine and Mitotracker. NBD-sphinganine labeled

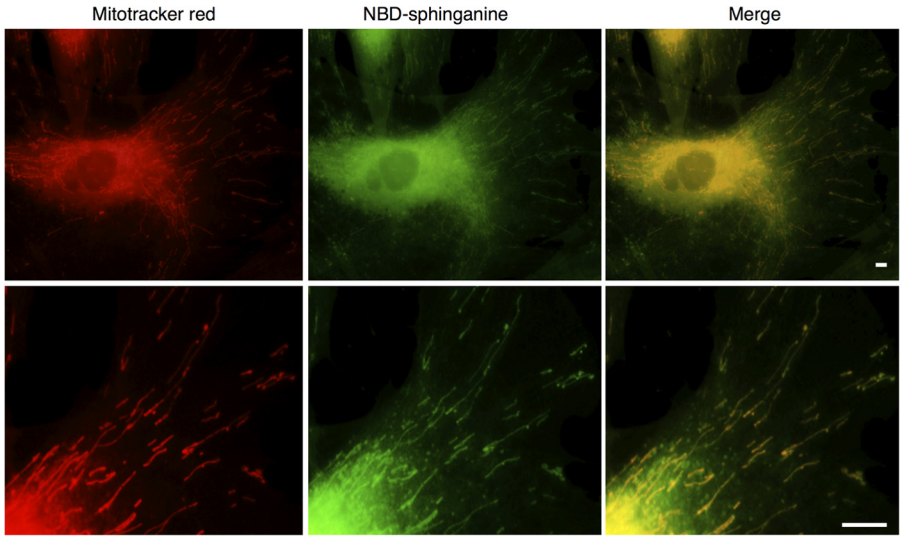

FIGURE 8. **NBD-sphinganine in mitochondria.** The distribution of NBD-sphinganine fluorescence was compared with that of Mitotracker red fluorescence. *Scale bar* = 10 μm; the *upper panels* show NBD-sphinganine distribution in a whole cell, and the *lower panels* show NBD-sphinganine in mitochondria. Data are from a representative experiment repeated three times.

a number of intracellular organelles including the mitochondria (Fig. 8). No metabolism of NBD-sphinganine occurred because cells were fixed before incubation. In addition, cells were incubated with the CerS inhibitor, fumonisin B1, before incubation with NBD-sphinganine, and an identical labeling pattern was observed.

Finally, we examined whether similar changes were observed in heart. In contrast to liver, no changes in the activity of any of the mitochondrial complexes were observed (Fig. 9*A*). Levels of very long chain ceramides were depleted, and there appeared to be a small increase in C16-ceramide, but the latter was not statistically significant (Fig. 9*B*). Sphingosine and sphinganine were also elevated (Fig. 9*C*) but to a much lower extent than in liver.

DISCUSSION

The main findings of the current study are that C16-ceramide, sphinganine, and possibly sphingosine modulate the mitochondrial respiratory chain by direct inhibition of complex IV. As a consequence, ROS are generated, which leads to chronic oxidative stress. We cannot exclude the possibility that other factors contribute to the elevation in ROS levels; however, the detection of ROS in mitochondria suggests that the mitochondrial electron transport chain is the primary source of ROS. It should be emphasized that the mechanism by which C16-ceramide levels are elevated (or, similarly, the mechanism by which C18-ceramide is elevated in brain (13)) is not known, but our current study demonstrates that this elevation is deleterious to the liver.

Although previous studies have demonstrated that ceramide can trigger ROS generation (41, 42), no studies are available comparing the role of ceramides with different natural acyl chain lengths on either the respiratory chain complex or on ROS generation. Studies are available examining the role of short acyl chain ceramide analogs (*i.e.* comparing C2- and C6-ceramide with C16-ceramide (42–44)), but these studies are limited because the short acyl chain analogs are very different in their biophysical properties to their long and very long acyl chain counterparts.

The role of ceramides with defined acyl chain lengths has received great attention over the past few years (3) in large part due to the discovery of the CerS (5) and due to the realization that mammalian cells expend significant effort regulating ceramide acyl chain composition. Specific ceramides are known to play defined roles in different signaling pathways (45, 46) and in cell pathologies, and we now add an additional pathway to this growing list by demonstrating that C16-ceramide, but not C24:0 or C24:1-ceramides, directly inhibit complex IV activity leading to ROS generation and oxidative stress. The specificity of the effect of C16-ceramide is further strengthened by the lack of effect of C16:0-C18:1-diacylglycerol. Both of these lipids have similar hydrophobic properties, but the lack of effect of the latter on complex IV demonstrates a specific mode of interaction between C16:0-ceramide and complex IV.

The mechanism by which C16:0-ceramide accesses complex IV in living mitochondria is currently unknown. There was considerable controversy concerning the role of SLs in mitochondria function (47), but recent studies measuring SL levels both in isolated mitochondria (48) and on isolation of enzymes of SL metabolism from mitochondria (49–52) have suggested that SLs are involved in regulation of mitochondrial function. This is supported by the involvement of the mitochondrial pathway in the pathology of a CERT-knock-out mouse (53). Unfortunately, no tools are available to determine the precise subcellular (or suborganellar) localization of long or very long chain ceramides. Recently, a fluorescent analog of sphinganine, NBD-sphinganine, has become available (54); sphinganine has been previously shown to inhibit complex IV activity and to increase ROS generation (43). Using NBD-sphinganine, we detected significant mitochondrial labeling in both live and fixed cells. Clearly, additional tools are required to determine the precise quantitative relationship between SLs/sphingoid long chain bases and mitochondria.

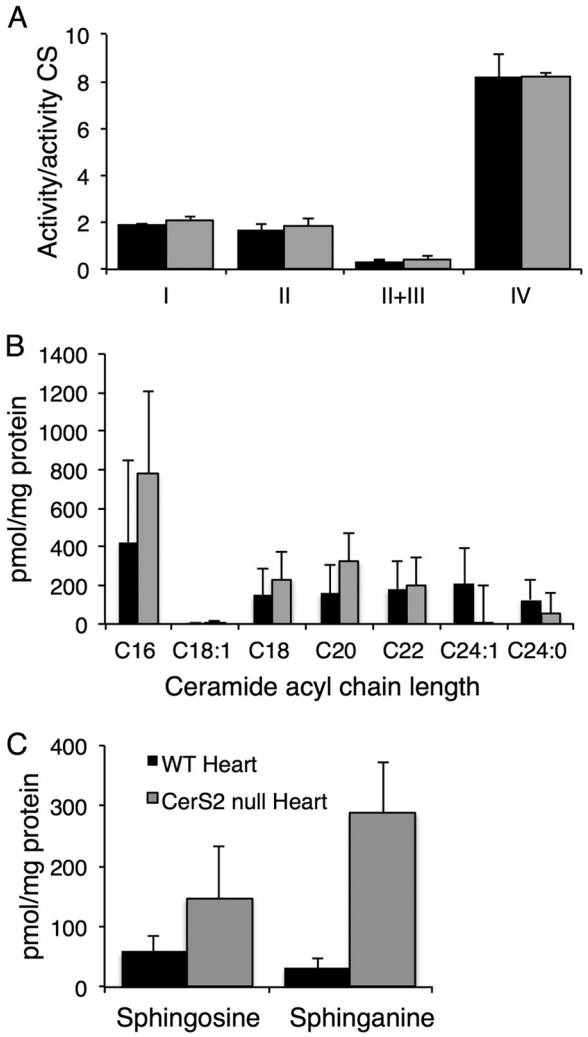

FIGURE 9. **Analysis of heart mitochondria isolated from CerS2 null mice.** *A*, shown are activities of mitochondrial complexes normalized to citrate synthase. Values are the means ± S.D., $n = 3$. *B* and *C*, shown is mass spectrometry analysis of ceramide acyl chain length (*B*) and sphingosine and sphinganine (*C*) in mitochondrial fractions from heart. Values are the means ± S.D., $n = 4$.

The mitochondrial inner membrane lipid composition is of importance for the stabilization of the respiratory chain complexes. This is exemplified by the fact that inborn errors of cardiolipin biosynthesis lead to diseases causing mitochondrial dysfunction (Barth syndrome) due to destabilization of the respiratory chain supercomplexes, specifically cytochrome *c* oxidase (55, 56). Despite the lack of detailed information about the mechanism by which sphinganine, sphingosine, and C16-ceramide gain access to complex IV in mitochondria, our data are consistent with the idea that their mode of interaction is highly specific and may involve competition with either the cytochrome *c* binding site or displacement of phospholipids that are bound to the enzyme (57).

CerS2 null mice display a progressive and severe hepatopathy. Our current results demonstrate that chronic oxidative stress in these mice may be responsible for some of this pathology. Attempts to reduce levels of ROS in cultured hepatocytes using antioxidants were successful, but this did not alter mitochondrial membrane potential. This implies that although oxidative stress plays a critical role in some pathological features, other mechanisms are at play that likely impact upon the hepatopathy of the CerS2 null mouse. Whether these other potential mechanisms are also related to direct interactions of C16-ceramide or sphinganine with specific pathways or, rather, are due to the lack of very long chain sphingolipids remains to be established.

Acknowledgments—We thank Drs. Shifra Ben-Dor and Ester Feldmesser for help with the digital gene expression analysis and Dr. Yuval Cinnamon for assistance with high resolution fluorescence microscopy.

REFERENCES

1. Futerman, A. H., and Hannun, Y. A. (2004) The complex life of simple sphingolipids. *EMBO Rep.* **5,** 777–782
2. Lahiri, S., and Futerman, A. H. (2007) The metabolism and function of sphingolipids and glycosphingolipids. *Cell. Mol. Life Sci.* **64,** 2270–2284
3. Hannun, Y. A., and Obeid, L. M. (2011) Many ceramides. *J. Biol. Chem.* **286,** 27855–27862
4. Reynolds, C. P., Maurer, B. J., and Kolesnick, R. N. (2004) Ceramide synthesis and metabolism as a target for cancer therapy. *Cancer Lett.* **206,** 169–180
5. Pewzner-Jung, Y., Ben-Dor, S., and Futerman, A. H. (2006) When do Lasses (longevity assurance genes) become CerS (ceramide synthases)? Insights into the regulation of ceramide synthesis. *J. Biol. Chem.* **281,** 25001–25005
6. Mullen, T. D., Hannun, Y. A., and Obeid, L. M. (2012) Ceramide synthases at the centre of sphingolipid metabolism and biology. *Biochem. J.* **441,** 789–802
7. Zhao, L., Spassieva, S. D., Jucius, T. J., Shultz, L. D., Shick, H. E., Macklin, W. B., Hannun, Y. A., Obeid, L. M., and Ackerman, S. L. (2011) A deficiency of ceramide biosynthesis causes cerebellar purkinje cell neurodegeneration and lipofuscin accumulation. *PLoS Genet.* **7,** e1002063
8. Ginkel, C., Hartmann, D., Vom Dorp, K., Zlomuzica, A., Farwanah, H., Eckhardt, M., Sandhoff, R., Degen, J., Rabionet, M., Dere, E., Dörmann, P., Sandhoff, K., and Willecke, K. (2012) Ablation of neuronal ceramide synthase 1 in mice decreases ganglioside levels and expression of myelin-associated glycoprotein in oligodendrocytes. *J. Biol. Chem.* **287,** 41888–41902
9. Jennemann, R., Rabionet, M., Gorgas, K., Epstein, S., Dalpke, A., Rothermel, U., Bayerle, A., van der Hoeven, F., Imgrund, S., Kirsch, J., Nickel, W., Willecke, K., Riezman, H., Gröne, H. J., and Sandhoff, R. (2012) Loss of ceramide synthase 3 causes lethal skin barrier disruption. *Hum. Mol. Genet.* **21,** 586–608
10. Pewzner-Jung, Y., Park, H., Laviad, E. L., Silva, L. C., Lahiri, S., Stiban, J., Erez-Roman, R., Brügger, B., Sachsenheimer, T., Wieland, F., Prieto, M., Merrill, A. H., Jr., and Futerman, A. H. (2010) A critical role for ceramide synthase 2 in liver homeostasis. I. alterations in lipid metabolic pathways. *J. Biol. Chem.* **285,** 10902–10910
11. Pewzner-Jung, Y., Brenner, O., Braun, S., Laviad, E. L., Ben-Dor, S., Feldmesser, E., Horn-Saban, S., Amann-Zalcenstein, D., Raanan, C., Berkutzki, T., Erez-Roman, R., Ben-David, O., Levy, M., Holzman, D., Park, H., Nyska, A., Merrill, A. H., Jr., and Futerman, A. H. (2010) A critical role for ceramide synthase 2 in liver homeostasis. II. Insights into molecular changes leading to hepatopathy. *J. Biol. Chem.* **285,** 10911–10923
12. Park, J. W., Park, W. J., Kuperman, Y., Boura-Halfon, S., Pewzner-Jung, Y., and Futerman, A. H. (2012) Ablation of very long acyl chain sphingolipids causes hepatic insulin resistance in mice due to altered detergent-resistant membranes. *Hepatology*, in press
13. Ben-David, O., Pewzner-Jung, Y., Brenner, O., Laviad, E. L., Kogot-Levin, A., Weissberg, I., Biton, I. E., Pienik, R., Wang, E., Kelly, S., Alroy, J., Raas-Rothschild, A., Friedman, A., Brügger, B., Merrill, A. H., Jr., and Futerman, A. H. (2011) Encephalopathy caused by ablation of very long acyl chain ceramide synthesis may be largely due to reduced galactosylceramide lev-

els. *J. Biol. Chem.* **286,** 30022–30033
14. Silva, L. C., Ben David, O., Pewzner-Jung, Y., Laviad, E. L., Stiban, J., Bandyopadhyay, S., Merrill, A. H., Jr., Prieto, M., and Futerman, A. H. (2012) Ablation of ceramide synthase 2 strongly affects biophysical properties of membranes. *J. Lipid Res.* **53,** 430–436
15. Yurlova, L., Kahya, N., Aggarwal, S., Kaiser, H. J., Chiantia, S., Bakhti, M., Pewzner-Jung, Y., Ben-David, O., Futerman, A. H., Brügger, B., and Simons, M. (2011) Self-segregation of myelin membrane lipids in model membranes. *Biophys. J.* **101,** 2713–2720
16. Raza, H. (2011) Dual localization of glutathione S-transferase in the cytosol and mitochondria. Implications in oxidative stress, toxicity, and disease. *FEBS J.* **278,** 4243–4251
17. Laskin, J. D., Black, A. T., Jan, Y. H., Sinko, P. J., Heindel, N. D., Sunil, V., Heck, D. E., and Laskin, D. L. (2010) Oxidants and antioxidants in sulfur mustard-induced injury. *Ann. N.Y. Acad. Sci.* **1203,** 92–100
18. Hayes, J. D., and Strange, R. C. (2000) Glutathione S-transferase polymorphisms and their biological consequences. *Pharmacology* **61,** 154–166
19. Turrens, J. F. (2003) Mitochondrial formation of reactive oxygen species. *J. Physiol.* **552,** 335–344
20. Dröge, W. (2002) Free radicals in the physiological control of cell function. *Physiol. Rev.* **82,** 47–95
21. Murphy, M. P., Holmgren, A., Larsson, N. G., Halliwell, B., Chang, C. J., Kalyanaraman, B., Rhee, S. G., Thornalley, P. J., Partridge, L., Gems, D., Nyström, T., Belousov, V., Schumacker, P. T., and Winterbourn, C. C. (2011) Unraveling the biological roles of reactive oxygen species. *Cell Metab.* **13,** 361–366
22. Mansat-de Mas, V., Bezombes, C., Quillet-Mary, A., Bettaïeb, A., D'orgeix, A. D., Laurent, G., and Jaffrézou, J. P. (1999) Implication of radical oxygen species in ceramide generation, c-Jun N-terminal kinase activation, and apoptosis induced by daunorubicin. *Mol. Pharmacol.* **56,** 867–874
23. Won, J. S., and Singh, I. (2006) Sphingolipid signaling and redox regulation. *Free Radic Biol. Med.* **40,** 1875–1888
24. Rigoulet, M., Yoboue, E. D., and Devin, A. (2011) Mitochondrial ROS generation and its regulation. Mechanisms involved in H_2O_2 signaling. *Antioxid. Redox Signal.* **14,** 459–468
25. Idkowiak-Baldys, J., Apraiz, A., Li, L., Rahmaniyan, M., Clarke, C. J., Kraveka, J. M., Asumendi, A., and Hannun, Y. A. (2010) Dihydroceramide desaturase activity is modulated by oxidative stress. *Biochem. J.* **427,** 265–274
26. Danial, N. N., Gramm, C. F., Scorrano, L., Zhang, C. Y., Krauss, S., Ranger, A. M., Datta, S. R., Greenberg, M. E., Licklider, L. J., Lowell, B. B., Gygi, S. P., and Korsmeyer, S. J. (2003) BAD and glucokinase reside in a mitochondrial complex that integrates glycolysis and apoptosis. *Nature* **424,** 952–956
27. Flock, G., Baggio, L. L., Longuet, C., and Drucker, D. J. (2007) Incretin receptors for glucagon-like peptide 1 and glucose-dependent insulinotropic polypeptide are essential for the sustained metabolic actions of vildagliptin in mice. *Diabetes* **56,** 3006–3013
28. Laviad, E. L., Albee, L., Pankova-Kholmyansky, I., Epstein, S., Park, H., Merrill, A. H., Jr., and Futerman, A. H. (2008) Characterization of ceramide synthase 2. Tissue distribution, substrate specificity, and inhibition by sphingosine 1-phosphate. *J. Biol. Chem.* **283,** 5677–5684
29. Sullards, M. C., and Merrill, A. H., Jr. (2001) Analysis of sphingosine 1-phosphate, ceramides, and other bioactive sphingolipids by high-performance liquid chromatography-tandem mass spectrometry. *Sci. STKE 2001*, pl1
30. Merrill, A. H., Jr., Sullards, M. C., Allegood, J. C., Kelly, S., and Wang, E. (2005) Sphingolipidomics. High throughput, structure-specific, and quantitative analysis of sphingolipids by liquid chromatography tandem mass spectrometry. *Methods* **36,** 207–224
31. Shaner, R. L., Allegood, J. C., Park, H., Wang, E., Kelly, S., Haynes, C. A., Sullards, M. C., and Merrill, A. H., Jr. (2009) Quantitative analysis of sphingolipids for lipidomics using triple quadrupole and quadrupole linear ion trap mass spectrometers. *J. Lipid Res.* **50,** 1692–1707
32. Saada, A., Shaag, A., and Elpeleg, O. (2003) mtDNA depletion myopathy. Elucidation of the tissue specificity in the mitochondrial thymidine kinase (TK2) deficiency. *Mol. Genet. Metab.* **79,** 1–5
33. Lowry, O. H., Rosebrough, N. J., Farr, A. L., and Randall, R. J. (1951) Protein measurement with the Folin phenol reagent. *J. Biol. Chem.* **193,** 265–275
34. Pedersen, P. L., Greenawalt, J. W., Reynafarje, B., Hullihen, J., Decker, G. L., Soper, J. W., and Bustamente, E. (1978) Preparation and characterization of mitochondria and submitochondrial particles of rat liver and liver-derived tissues. *Methods Cell Biol.* **20,** 411–481
35. Degli Esposti, M. (2002) Measuring mitochondrial reactive oxygen species. *Methods* **26,** 335–340
36. Saada, A., Bar-Meir, M., Belaiche, C., Miller, C., and Elpeleg, O. (2004) Evaluation of enzymatic assays and compounds affecting ATP production in mitochondrial respiratory chain complex I deficiency. *Anal. Biochem.* **335,** 66–72
37. Preethy, C. P., Padmapriya, R., Periasamy, V. S., Riyasdeen, A., Srinag, S., Krishnamurthy, H., Alshatwi, A. A., and Akbarsha, M. A. (2012) Antiproliferative property of *n*-hexane and chloroform extracts of *Anisomeles malabarica* (L). R. Br. in HPV16-positive human cervical cancer cells. *J. Pharmacol. Pharmacother.* **3,** 26–34
38. Pagano, R. E., Sepanski, M. A., and Martin, O. C. (1989) Molecular trapping of a fluorescent ceramide analogue at the Golgi apparatus of fixed cells. Interaction with endogenous lipids provides a trans-Golgi marker for both light and electron microscopy. *J. Cell Biol.* **109,** 2067–2079
39. Mattson, M. P. (2009) Roles of the lipid peroxidation product 4-hydroxynonenal in obesity, the metabolic syndrome, and associated vascular and neurodegenerative disorders. *Exp. Gerontol.* **44,** 625–633
40. Hoff, H. F., and O'Neil, J. (1993) Structural and functional changes in LDL after modification with both 4-hydroxynonenal and malondialdehyde. *J. Lipid Res.* **34,** 1209–1217
41. Li, X., Becker, K. A., and Zhang, Y. (2010) Ceramide in redox signaling and cardiovascular diseases. *Cell. Physiol. Biochem.* **26,** 41–48
42. Di Paola, M., Cocco, T., and Lorusso, M. (2000) Ceramide interaction with the respiratory chain of heart mitochondria. *Biochemistry* **39,** 6660–6668
43. García-Ruiz, C., Colell, A., Marí, M., Morales, A., and Fernández-Checa, J. C. (1997) Direct effect of ceramide on the mitochondrial electron transport chain leads to generation of reactive oxygen species. Role of mitochondrial glutathione. *J. Biol. Chem.* **272,** 11369–11377
44. Gudz, T. I., Tserng, K. Y., and Hoppel, C. L. (1997) Direct inhibition of mitochondrial respiratory chain complex III by cell-permeable ceramide. *J. Biol. Chem.* **272,** 24154–24158
45. Stiban, J., Tidhar, R., and Futerman, A. H. (2010) Ceramide synthases. Roles in cell physiology and signaling. *Adv. Exp. Med. Biol.* **688,** 60–71
46. Kroesen, B. J., Jacobs, S., Pettus, B. J., Sietsma, H., Kok, J. W., Hannun, Y. A., and de Leij, L. F. (2003) BcR-induced apoptosis involves differential regulation of C16 and C24-ceramide formation and sphingolipid-dependent activation of the proteasome. *J. Biol. Chem.* **278,** 14723–14731
47. Futerman, A. H. (2006) Intracellular trafficking of sphingolipids. Relationship to biosynthesis. *Biochim. Biophys. Acta* **1758,** 1885–1892
48. Ardail, D., Popa, I., Alcantara, K., Pons, A., Zanetta, J. P., Louisot, P., Thomas, L., and Portoukalian, J. (2001) Occurrence of ceramides and neutral glycolipids with unusual long-chain base composition in purified rat liver mitochondria. *FEBS Lett.* **488,** 160–164
49. Novgorodov, S. A., Wu, B. X., Gudz, T. I., Bielawski, J., Ovchinnikova, T. V., Hannun, Y. A., and Obeid, L. M. (2011) Novel pathway of ceramide production in mitochondria. Thioesterase and neutral ceramidase produce ceramide from sphingosine and acyl-CoA. *J. Biol. Chem.* **286,** 25352–25362
50. El Bawab, S., Roddy, P., Qian, T., Bielawska, A., Lemasters, J. J., and Hannun, Y. A. (2000) Molecular cloning and characterization of a human mitochondrial ceramidase. *J. Biol. Chem.* **275,** 21508–21513
51. Shimeno, H., Soeda, S., Sakamoto, M., Kouchi, T., Kowakame, T., and Kihara, T. (1998) Partial purification and characterization of sphingosine *N*-acyltransferase (ceramide synthase) from bovine liver mitochondrion-rich fraction. *Lipids* **33,** 601–605
52. Bionda, C., Portoukalian, J., Schmitt, D., Rodriguez-Lafrasse, C., and Ardail, D. (2004) Subcellular compartmentalization of ceramide metabolism. MAM (mitochondria-associated membrane) and/or mitochondria? *Biochem. J.* **382,** 527–533
53. Wang, X., Rao, R. P., Kosakowska-Cholody, T., Masood, M. A., Southon, E., Zhang, H., Berthet, C., Nagashim, K., Veenstra, T. K., Tessarollo, L.,

Acharya, U., and Acharya, J. K. (2009) Mitochondrial degeneration and not apoptosis is the primary cause of embryonic lethality in ceramide transfer protein mutant mice. *J. Cell Biol.* **184,** 143–158
54. Kim, H. J., Qiao, Q., Toop, H. D., Morris, J. C., and Don, A. S. (2012) A fluorescent assay for ceramide synthase activity. *J. Lipid Res.* **53,** 1701–1707
55. Vreken, P., Valianpour, F., Nijtmans, L. G., Grivell, L. A., Plecko, B., Wanders, R. J., and Barth, P. G. (2000) Defective remodeling of cardiolipin and phosphatidylglycerol in Barth syndrome. *Biochem. Biophys. Res. Commun.* **279,** 378–382
56. Böttinger, L., Horvath, S. E., Kleinschroth, T., Hunte, C., Daum, G., Pfanner, N., and Becker, T. (2012) Phosphatidylethanolamine and cardiolipin differentially affect the stability of mitochondrial respiratory chain supercomplexes. *J. Mol. Biol.* **423,** 677–686
57. Hasinoff, B. B., and Davey, J. P. (1989) The inhibition of a membrane-bound enzyme as a model for anaesthetic action and drug toxicity. *Biochem. J.* **258,** 101–107
58. Voss, K. A., Liu, J., Anderson, S. P., Dunn, C., Miller, J. D., Owen, J. R., Riley, R. T., Bacon, C. W., and Corton, J. C. (2006) Toxic effects of fumonisin in mouse liver are independent of the peroxisome proliferator-activated receptor α. *Toxicol. Sci.* **89,** 108–119
59. Hardman, M. J., Emmerson, E., Campbell, L., and Ashcroft, G. S. (2008) Selective estrogen receptor modulators accelerate cutaneous wound healing in ovariectomized female mice. *Endocrinology* **149,** 551–557